JOURNAL OF SPACECRAFT AND ROCKETS
Vol. 32, No. 1, January–February 1995

Numerical Analysis of Hypersonic Low-Density Scramjet Inlet Flow

Chan H. Chung* and Suk C. Kim†
NASA Lewis Research Center, Cleveland, Ohio 44135
Kenneth J. De Witt‡
University of Toledo, Toledo, Ohio 43606
and
Henry T. Nagamatsu§
Rensselaer Polytechnic Institute, Troy, New York 12180

Hypersonic low-density flow around a two-dimensional scramjet inlet model has been analyzed using the direct simulation Monte Carlo (DSMC) method. The predominant features of hypersonic flows, such as a thick viscous layer due to the low-density fluid together with shock–boundary-layer interaction and shock impingement as well as shock-induced separation, are encountered in this type of flowfield. Three hypersonic flowfields with different degrees of rarefaction are investigated. The freestream Knudsen numbers of the flowfields based on the height of the duct passage are in the range of 0.02–0.12. Conventional continuum gasdynamics based on the concept of a local equilibrium may not be adequate to describe this type of flowfield accurately. The pressures obtained by the DSMC simulation are compared with available experimental data. Good agreement is obtained with previous experimental data and with theoretical solutions for similar wedge flow cases near the leading edge of the ramp centerbody. Good agreement is observed with the experimental data of Minucci and Nagamatsu except for some discrepancies, especially in the lower-density cases, which may be partially attributed to three-dimensional effects and/or to experimental uncertainty.

Nomenclature

C^* = modified Chapman-Rubesin constant defined in Eq. (1)
d = height of duct passage, mm
Kn = Knudsen number, λ_∞/d
M = Mach number
P = pressure, Pa
Re_x = local Reynolds number, $\rho_\infty U_\infty x/\mu_\infty$
T = temperature, K
U = flow velocity, m/s
x, y = coordinates, mm
α = angle of attack in freestream uniform flow, deg
γ = ratio of specific heats
θ = wedge angle, deg
λ = mean free path, mm
μ = viscosity, N/m·s
ρ = density, kg/m^3
ω = VHS exponent

Subscripts

p = pitot pressure
W = wall condition
0 = stagnation condition
∞ = freestream condition

Superscript

$*$ = reference condition

Presented as Paper 93-2870 at the AIAA 28th Thermophysics Conference, Orlando, FL, July 6–9, 1993; received July 20, 1993; revision received March 4, 1994; accepted for publication March 4, 1994.

*Resident Research Associate. Member AIAA.
†Senior Research Engineer, NYMA, Inc., Lewis Research Center Group. Member AIAA.
‡Professor, Department of Chemical Engineering, Member AIAA.
§Professor, Department of Aeronautical Engineering. Fellow AIAA.

Introduction

THE understanding of hypersonic low-density flows is very important for the development of vehicles designed to operate at very high altitudes, such as the National Aerospace Plane (NASP) and orbital transfer vehicles (OTVs). In hypersonic flows, viscous interaction is a key phenomenon, that governs the structure of the flow around any configuration.

In the flows around vehicles operating at high altitudes, the Reynolds number becomes smaller on account of the low density, and the effect of the viscous interaction becomes more significant. Also, as the freestream density decreases, rarefaction effects such as surface slip and various nonequilibrium effects must be taken into account for the accurate analysis of the flow. Consequently, conventional continuum gasdynamics, which is based on the concept of a local equilibrium, may not be adequate, and an approach based on molecular gasdynamics is required. Of the various methods for the analysis of low-density flows, the direct simulation Monte Carlo (DSMC) methods developed by Bird[1] is the one that is most widely used and readily applicable to complex problems. The DSMC method is a computer simulation technique to solve Boltzmann's equation by modeling a real gas flow using a representative set of molecules. Theoretically, the DSMC method can be applied to any flows for which Boltzmann's equation is valid. Its ability to handle complex flows with the effect of strong viscous interaction has been demonstrated, for example, through application to a compression corner flow by Moss et al.[2] and to a complex shock interaction problem by Carlson and Wilmoth.[3]

In the present study, hypersonic low-density flow around a scramjet inlet model has been analyzed using the DSMC method. This type of flow is characterized by a thick viscous layer due to the low-density fluid that occupies most of the inlet capture streamtube. Also, shock–boundary-layer interaction, shock impingement, and shock-induced separation are dominant features of hypersonic flows. Extensive computational studies of the flowfields around a scramjet inlet have been conducted using conventional continuum methods, but less attention has been devoted to the strong viscous-inviscid interaction with merged regions of the shock wave and boundary layer in hypersonic low-density flows. An accurate analysis of this type

of flow structure associated with the ingestion of the thick viscous layer by the inlet is especially important in determining the inlet performance of high-speed vehicles at very high altitudes.

The aim of the present study is to reproduce numerically the experimental flowfields that have been measured at Rensselaer Polytechnic Institute[4] in a hypersonic shock-tube tunnel using dry air as a test gas. The inlet model employed in the experiment is 322 mm long and 40.35 mm high, and consists of a long inlet ramp, a straight duct passage formed by a short cowl, and an exhaust in the rear section of the model, which is a typical configuration of aerospace vehicles operating in hypersonic flow regimes.

In the experiment, a series of test cases was investigated corresponding to two flow conditions, referred to as low- and high-enthalpy air, with stagnation temperatures of 1100 and 4100 K, respectively. The low-enthalpy case was investigated by Lai et al.[5] by using a continuum method, the PARC code.[6,7] In the present work, the high-enthalpy case is considered, for which continuum solutions are not available. Calculations are made for a two-dimensional scramjet inlet model at three Mach numbers, 12, 15, and 18. The corresponding freestream Knudsen numbers based on the height of the duct passage are in the range of 0.02–0.12. The numerical results are compared with experimental data in which wall pressures along the ramp center body and cowl surfaces are measured together with the pitot pressure across the duct passage near the cowl's blunt trailing edge.

Inlet Model

The scramjet inlet model tested in the experiment and in the present numerical analysis is shown in Fig. 1. The scramjet model, 322 mm long and 40.35 mm high, consists of a long centerbody, which is usually integrated as an undersurface of aerospace vehicles, and an upper cowl designed relatively short to reduce the vehicle's weight. These two surfaces form an inlet comprising a compression ramp, extending slightly beyond the sharp cowl lip together with a straight duct passage ending at the cowl blunt trailing edge and the centerbody second expansion corner. The arrangement also allows for an exhaust flow in the rear section, representing a typical scramjet nozzle using part of the centerbody as its only expanding surface. This is a typical configuration of aerospace vehicles operating in hypersonic regimes. In Fig. 1, all dimensions indicated are in millimeters. The maximum thicknesses of the centerbody and the cowl are 18.8 and 16.25 mm, respectively. The region enveloped by dashed lines ($ABCDEF$) represents the computational domain. The lines AB, BC, and AF are freestream inflow boundaries, and the lines CD and EF are supersonic outflow boundaries. The upstream inflow boundary AB is moved upstream to where the flow is not disturbed by the flow around the ramp leading edge. The freestream boundary conditions along the upper inflow boundary BC are imposed at a distance sufficiently far from the inlet model where the ramp external shock does not intersect. The angle of attack in the freestream uniform flow, α, is assumed to be 0 deg. The freestream gas is air with a stagnation temperature of 4100 K. The freestream flow conditions are shown in Table 1. The wall was assumed to be at a constant temperature of 300 K, which is room temperature in the experiment.

Table 1 Freestream flow conditions

	M_∞	T_∞, K	ρ_∞, 10^{-4} kg/m^3	P_∞, Pa	$Kn = \lambda_\infty/d$
Case I	12.0	208.0	1.89	11.0	0.02
Case II	15.0	135.0	0.64	2.4	0.06
Case III	18.0	94.3	0.26	0.68	0.12

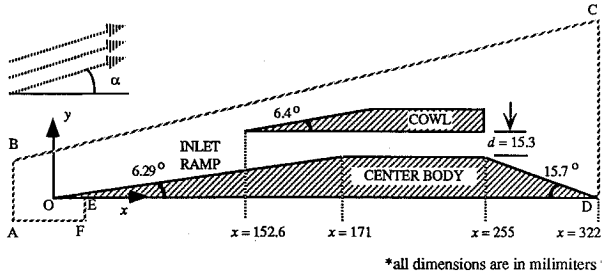

Fig. 1 Geometry of the scramjet inlet model.

DSMC Method

The DSMC method is a popular simulation technique for low-density flows, and the DSMC code used in the present study is based on the same principles as described in Bird,[1] together with the variable hard-sphere (VHS) model[8] as a molecular model and the no-time counter (NTC) method[9] as a collision sampling technique. The code was developed at the NASA Lewis Research Center and has been used to investigate various low-density flows.[10–12] In the code, the flow domain is divided into several subregions, and the cell structure in each region is constructed by analytical grid transformations so that an exact molecular indexing can be done by a simple algebraic equation rather than by fuzzy point indexing.[1] The code is fully vectorized to utilize the now-popular vector computers. General ideas regarding vectorization of the DSMC method can be found in Usami et al.[13] and Boyd.[14] The total CPU time required for the flow considered in the present study is in a range of 12–16 h on a Cray Y/MP supercomputer, and the execution speed of the code, which is measured by CPU time per particle per timestep, is about 1.3–1.8 μs, depending on the freestream condition.

The computational flow domain consists of about 45,000–60,000 cells, depending on the freestream condition, in 48 subregions. The cell size is kept less than the local mean free path in both the x and y directions except for case I, in which some cells inside the duct passage are about 2–4 times larger than the local mean free path in the x direction. At the steady phase of the simulation, the total number of simulated molecules in the flow domain is about 1–1.5 million, depending on the freestream condition. The flowfield is sampled every 5 timesteps during 20,000 timesteps after reaching the steady phase. The transient phase, in which the solution develops and the flow structures form, is accelerated by employing one-fourth the usual number of simulated particles and a four times larger timestep than that for the steady phase. Then, all the simulated molecules in the flow domain are cloned, as was done in McDonald.[15] Before commencing the sampling, about 6000 timesteps are run through to allow the complex flow structures to be fully developed and to prevent any deleterious effects in the final results due to the cloning.

The freestream fluid is modeled as air in equilibrium corresponding to the freestream condition[16] with 79% nitrogen and 21% oxygen by volume. The VHS exponent ω of the gas mixture is chosen to be 0.25. The reference molecular diameters of nitrogen and oxygen are chosen to be 4.07×10^{-10} and 3.96×10^{-10}m, respectively, at a reference temperature of 2.73 K. Chemical reactions are assumed to be frozen. For the calculation of rotational and vibrational energy exchange between the colliding molecules, the Borgnakke-Larsen phenomenological model[17] is employed. A diffusely reflecting wall with full accommodation at the wall temperature is assumed for the interaction between the gas molecules and the wall. The probabilities of rotational and vibrational energy exchange were chosen to be 0.2 and 0.02, respectively. The wall is assumed to be a monatomic gas with an infinite mass for the internal-translational energy exchange of the reflecting molecules, and the probabilities are assumed to be the same as those in the gas mixture.

Results and Discussion

To present the overall structure of the flowfield in the present scramjet model and the behavior of the low-density flows, Mach-number and pressure contours obtained by the DSMC method will be considered first. Figure 2 shows Mach-number contours for case I, in which the freestream Mach number is $M_\infty = 12$. Highly oblique shock waves and thick viscous layers are predominant features of the flowfield. In the figure, the difference in Mach number between adjacent contours is 0.5. It can be seen that the sharp ramp shock does not impinge on the internal surface of the cowl, but passes above the cowl leading edge to be deflected at a larger angle around the cowl leading edge on the external surface. The ramp boundary layer grows to a thickness equal to the height of the duct passage, and directly interacts with the cowl leading edge. The cowl leading-edge shock is completely immersed in the boundary layer.

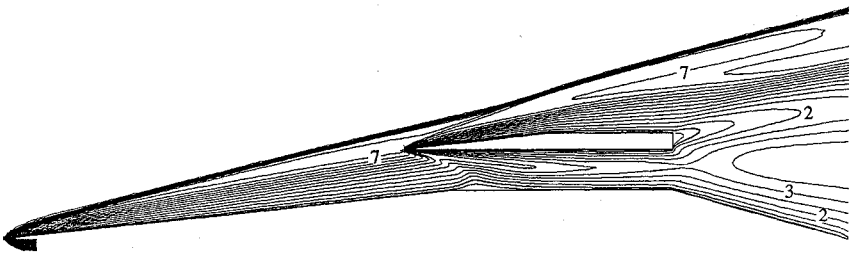

Fig. 2 Mach-number contours, $M_\infty = 12$.

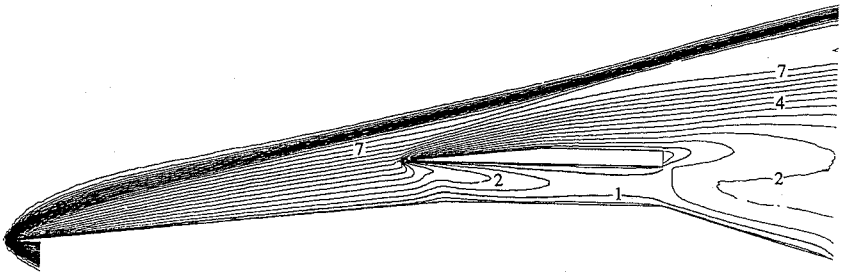

Fig. 3 Mach-number contours, $M_\infty = 15$.

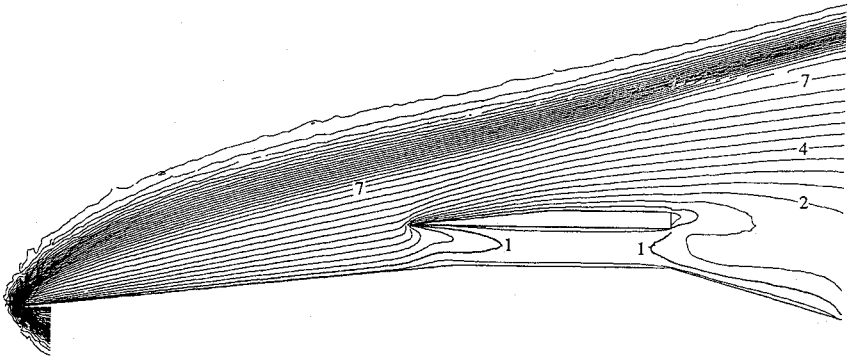

Fig. 4 Mach-number contours, $M_\infty = 18$.

Upon impinging upon the centerbody surface near the juncture, the cowl leading-edge shock causes flow separation. In the region behind the cowl blunt trailing edge, the flow structure becomes complex, involving viscous-dominated flows followed by a mixing shear layer occurring between two hypersonic streams.

Figure 3 shows Mach-number contours for case II, in which the freestream Mach number is $M_\infty = 15$. The freestream Knudsen number for case II is about 3 times larger than that in case I. It can be seen that the ramp leading-edge shock is not as sharp as that in case I. The ramp boundary layer grows more than 1.5 times thicker than the height of the duct passage at the cowl leading edge. The cowl leading-edge shock inside the duct passage also becomes diffusive. Inside the duct passage, the subsonic layer grows to more than half the height of the passage near the rear end. All of these phenomena are due to the increase of the mean free path.

The effect of rarefaction can be seen more clearly in Fig. 4, which shows Mach-number contours for case III. The freestream mean free path in case III is about 2 times larger than that in case II. It can be seen that the ramp leading-edge shock becomes diffusive and the ramp boundary layer grows to more than 2 times the height of the duct passage at the cowl leading edge. The duct passage is filled with the subsonic layer. This is because, as the mean free path increases, the effect of molecule-surface collisions becomes more important than that of molecule-molecule collisions. Molecules near the wall that have experienced a collision with the surface can travel further without suffering from molecule-molecule collisions. This means that the effect of the existence of the surface increases.

More detailed flow structure inside the duct passage can be seen in Fig. 5, in which pressure contours are plotted for the case of freestream Mach number $M_\infty = 12$. The pressure is the average value of the pressures in the x, y, and z directions and is normalized by the freestream pressure. The interaction of the cowl leading-edge shock with the ramp boundary layer can be clearly seen. The cowl leading-edge shock is reflected at the ramp centerbody surface toward the rear end of the cowl with a small positive angle, to be dissipated by the exhaust flow. As the freestream mean free path becomes larger, the interaction of the cowl leading-edge shock with the ramp boundary layer becomes more diffusive, as can be seen in Figs. 6 and 7, which show pressure contours for the cases of freestream Mach number $M_\infty = 15$ and 18, respectively. The location at the centerbody surface on which the cowl leading-edge shock impinges moves forward because of the increase of the shock angle. It also can be seen in the figures that the flow in the rear part of the duct passage becomes almost symmetric because of the increase of the wall effect as the flow becomes more rarefied.

Consideration is now given to the nonequilibrium phenomena in the flow. Figure 8 shows translational and internal temperature variations along the ramp centerbody surface for case I. The internal temperature consists of rotational and vibrational temperatures. It can be seen that the flow is in a highly thermal nonequilibrium state. The translational temperature shows a sudden increase, a peak value of about 3500 K while passing through the shock and then a decrease to about 1000 K. It gradually decreases to about 600 K because of the cold wall at 300 K. The internal temperature also

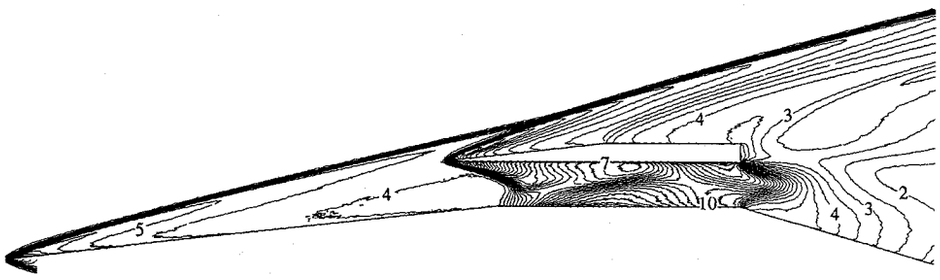

Fig. 5 Pressure contours, $M_\infty = 12$.

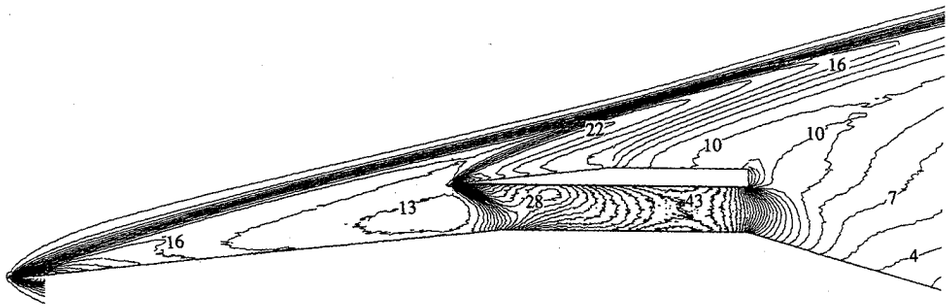

Fig. 6 Pressure contours, $M_\infty = 15$.

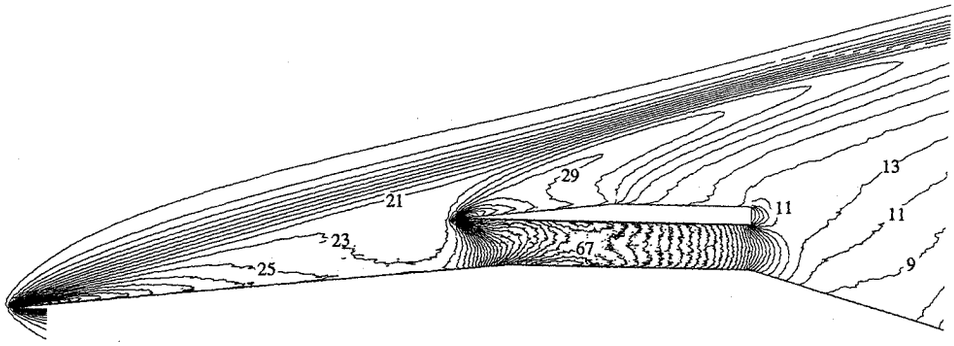

Fig. 7 Pressure contours, $M_\infty = 18$.

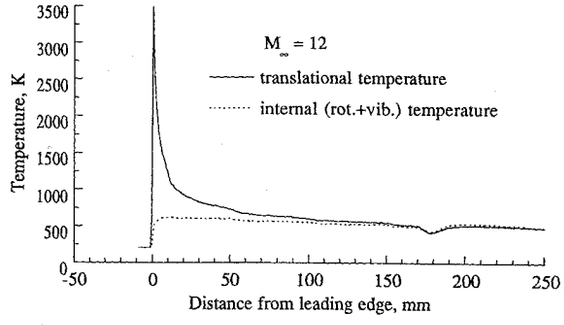

Fig. 8 Temperature variation along the ramp centerbody surface.

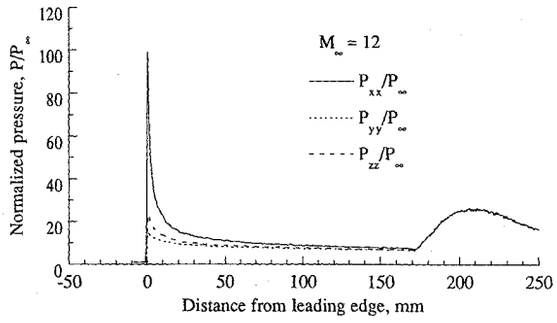

Fig. 9 Pressure variation along the ramp centerbody surface.

jumps to around 700 K while passing through the shock, and then gradually decreases to equilibrate with the translational temperature. Both temperatures show a minimum around the separation point due to the increased interaction with the cold surface. A severe translational nonequilibrium also exists in the flow, as can be seen in Fig. 9, in which pressures in the x, y, and z directions along the ramp centerbody surface for case I are shown. The pressures are calculated by the equation of state. It can be seen that the magnitudes of pressures in each direction are different, especially near the ramp leading edge, because of the strong nonequilibrium and large slip.

Hypersonic low-density flowfields for a flat plate or wedge are subjects of classical interest and have been studied previously by many investigators, both theoretically and experimentally. Since the ramp of the present inlet model is a wedge with a wedge angle of $\theta = 6.29$ deg, it would be interesting to compare the DSMC results with the previous experimental data of Vidal and Bartz[18] together with those of Minucci and Nagamatsu.[4] The behavior of the surface

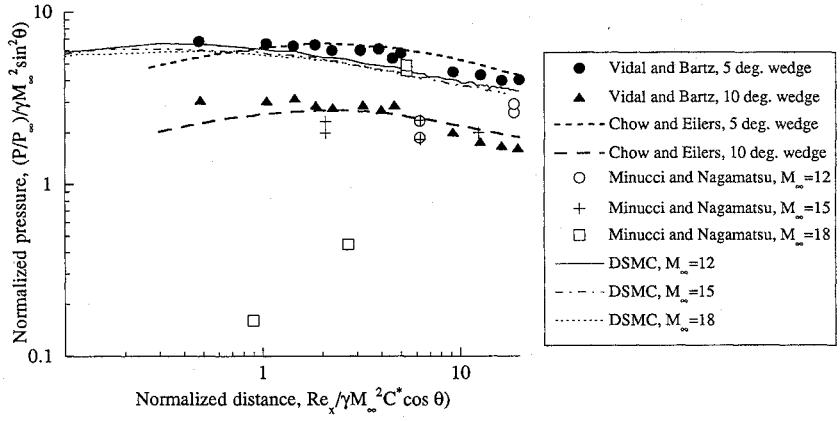

Fig. 10 Comparison of surface pressure along the ramp centerbody surface.

pressure around the leading edge in the results of the present DSMC simulation is more consistent with those observed by previous investigators. Figure 10 shows comparison of surface pressures along the ramp centerbody. The DSMC pressures are obtained by calculating the normal force per unit area on the surface exerted by colliding molecules. In the figure, the vertical axis is the normalized surface pressure by the Newton-Buseman approximation for wedge pressure, and the abscissa is the normalized distance used by Vidal and Bartz. The quantity C^* is the modified Chapman-Rubesin constant,[18] which is defined by

$$C^* = \frac{\mu^*}{\mu_\infty}\frac{T_\infty}{T^*} \tag{1}$$

where μ^* is the viscosity at a reference temperature T^* given by

$$\frac{T^*}{T_0} = \frac{1}{6} + \frac{1}{2}\frac{T_W}{T_0} \tag{2}$$

The experimental data of Vidal and Bartz are for wedges with wedge angles $\theta = 5$ and 10 deg in a dry-air flow with stagnation temperature 4000 K and surface temperature 300 K, which are similar conditions to those in the present problem. The freestream Mach numbers are in the range of 19–20.8. The corresponding freestream unit Reynolds numbers are in the range of $(1.1–8.5) \times 10^4$/m, and are also closer to those in the present problem, $(1.4–4.6) \times 10^4$/m. It can be seen that the present DSMC results lie between the results for the 5- and 10-deg wedges of Vidal and Bartz. Also, the present DSMC results and the experimental data of Vidal and Bartz are in good agreement with the theory of Chow and Eilers.[19] The experimental data of Minucci and Nagamatsu show much lower values than those for the 10-deg wedge of Vidal and Bartz, especially in the high-Mach-number case.

In the experiment, the air was expanded through a 30-deg-included conical nozzle with an exit diameter of 60 cm. The leading edge of the inlet model was located 15 mm downstream from the nozzle exit. Hence, there is a possibility that the freestream may not be uniform with a 0-deg flow angle. In addition, vibration of the model could result in a slight misalignment with the freestream. Hence, the flowfields are calculated for both $\alpha = 0$ and 2.5 deg. It is found that the ramp centerbody surface pressure is very sensitive to the freestream angle of attack.

In Figs. 11–13, the wall pressure at the ramp centerbody surface is plotted from the entrance to the rear end of the duct passage. The pressure is normalized by the freestream pitot pressure. The results from the DSMC method for $\alpha = 0$ deg show 25–30% higher wall pressure than the experimental data. The results show a maximum inside the duct passage, which corresponds to the location on which the cowl leading-edge shock impinges. As the gas becomes rarefied, the peak moves forward because of the increase in the cowl leading-edge shock angle. In the case of $M_\infty = 15$, the DSMC pressure is double-peaked, and the second peak is due to the arrival of the very weak shock that has been reflected at the cowl surface. As the gas becomes even more rarefied, the shock becomes very weak

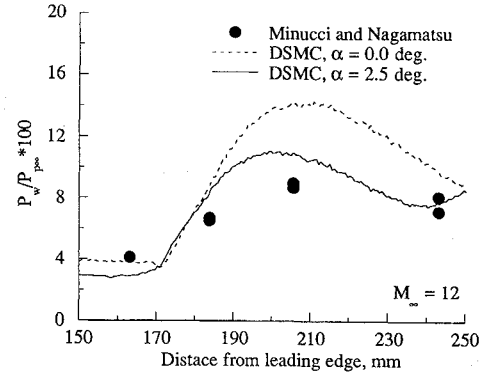

Fig. 11 Comparison of surface pressure along the ramp centerbody in the duct passage.

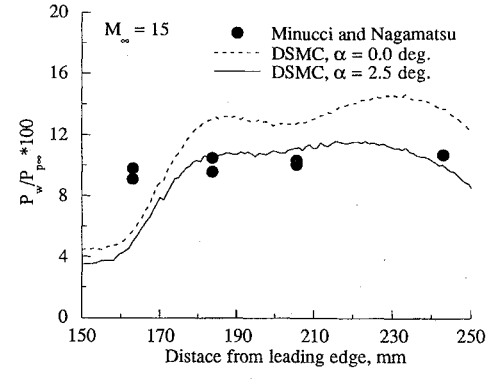

Fig. 12 Comparison of surface pressure along the ramp centerbody in the duct passage.

and diffusive, as can be seen in Fig. 13. The DSMC results for $\alpha = 2.5$ deg are also shown in Figs. 11–13. It can be seen that the freestream condition with $\alpha = 2.5$ deg gives better agreement with the experiment. It is interesting to see, in the case of $M_\infty = 12$, that the peak moves forward because of the increase in the cowl leading-edge shock angle and the secondary peak starts to appear at the rear part of the duct because of the secondary arrival of the very weak shock. In Figs. 14–16, the wall pressure on the cowl surface is plotted from the entrance to the rear end of the duct passage. The secondary peaks in the pressure profiles are caused by the arrival of the weakened cowl leading-edge shock reflected from the centerbody. Again, it can be seen that an angle of attack of 2.5 deg gives better agreement with the experiment except for $M_\infty = 18$.

There are several other possibilities that may result in the discrepancy between the DSMC results and the experimental data. These include three-dimensional effects, an orifice effect due to rarefaction, and chemical nonequilibrium. These possibilities will be discussed below.

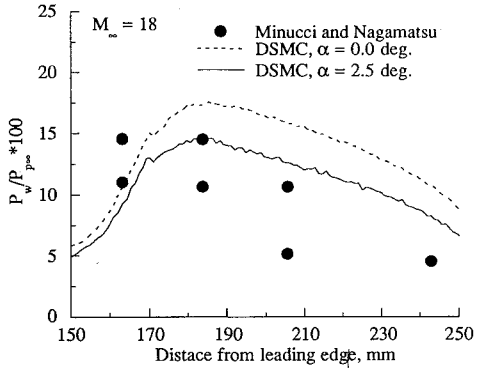

Fig. 13 Comparison of surface pressure along the ramp centerbody in the duct passage.

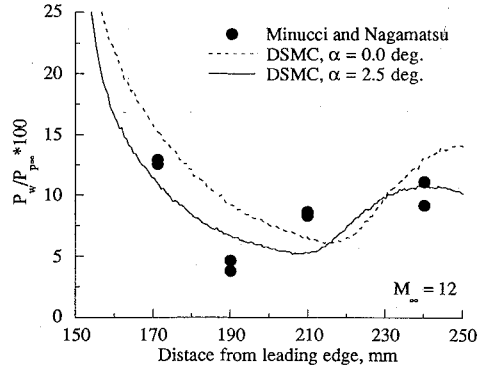

Fig. 14 Comparison of surface pressure along the cowl in the duct passage.

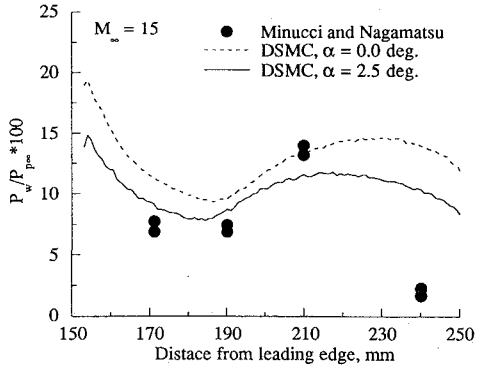

Fig. 15 Comparison of surface pressure along the cowl in the duct passage.

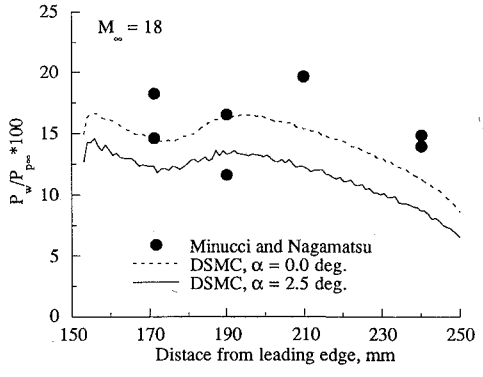

Fig. 16 Comparison of surface pressure along the cowl in the duct passage.

In the inlet model, the ratio of the width to the height of the duct passage is about 16.3. The continuum calculation of Lai et al.[5] for the low-enthalpy case implies that a relieved spillage effect can be produced by an ambient pressure that is lower than the pressure on the centerbody surface. The continuum results showed that the three-dimensional effects were negligible for $M_\infty = 12$, but have some effect for $M_\infty = 19.1$. In the continuum results obtained for $M_\infty = 19.1$, the location of the maximum wall pressure inside the duct passage is shifted downstream, whereas the maximum value is not affected. Also, the convergence for this case was only marginal and could not be achieved for lower-density cases, owing the drastically thickened ramp boundary layer. This means that the possibility of three-dimensional effects must be viewed with caution.

In low-density flows, the true pressure on a surface can be different from that measured in orifice cavities or pressure holes, because of the increase in the effect of molecule-surface collisions, which is called an "orifice effect."[20] The orifice effect can significantly affect the pressure data measured by using pressure holes in low-density flows. The best way to avoid this complication is to use a pressure gauge that has its sensing element flush with the wall. In the experiment of Minucci and Nagamatsu, pressure taps that are 1.7 mm in diameter and about 1.5 mm in depth were used to install pressure transducers at the bottom of the tap.[16] The dimensions of these pressure taps are comparable with the mean free path of the flowfield near the leading edge, and the measured wall pressure near the leading edge should have been affected by the orifice effect, while the effect becomes negligible inside the duct passage. The assessment of the orifice effect for the experiment of Minucci and Nagamatsu is a formidable task as a result of the combined effect of thermal nonequilibrium, shear stress, internal energy, and tab geometry.[21] An alternative way to assess the effect is to simulate the three-dimensional flowfield with many pressure holes using the DSMC method, but that is computationally prohibitive at the present time.

In the present study, chemical reactions are assumed to be frozen because the wall is at the room temperature of 300 K. Although not shown, the translational temperature in most of the flowfield obtained by the DSMC method was less than 2300 K except for extremely small regions near the leading edges of the ramp centerbody and the cowl, where the maximum translational temperature goes up to 4000 K. The internal temperature in most of the flowfield was less than 2000 K. Consequently, the temperature of the air in most of the flowfield was less than 2200 K except for the extremely small region near the leading edges of the ramp centerbody and the cowl, where the maximum temperature goes up to 2400 K. At this condition, dissociation of oxygen would be negligible. This justifies the assumption of frozen chemistry.

Finally, pitot pressure distributions across the duct passage at a location $x = 247.7$ mm for $M_\infty = 12$ and 15, respectively, are shown in Fig. 17. Again, the pitot pressures are normalized by the freestream pitot pressure. It can be seen that the pitot pressure decreases as the flow becomes rarefied, because of the increase of the effect of molecule-surface collisions, i.e., increase of the effect of the cold wall, as was mentioned earlier. The pitot pressures obtained by the DSMC method for $\alpha = 0$ deg show significantly higher values than the experimental data, especially for $M_\infty = 15$, which may be partially attributed to the effect of rarefaction. It is well known[20] that, in low-density flows, measured pitot pressures do not coincide with the ideal impact pressure, which is also a kind of orifice effect as discussed earlier. The difference between the two pressures becomes larger as the flow becomes more rarefied and the probe diameter becomes smaller. In the experiment of Minucci and Nagamatsu, a thin-walled stainless steel tube with a internal diameter of 1.5 mm was used.[16] The diameter of the tube is comparable with the mean free path of the flowfield, and the ideal pitot pressures obtained by the DSMC method need to be corrected in order to be directly comparable with the measured impact pressures. The DSMC impact pitot pressures corrected by using experimental data compiled by Fisher[22] are also shown in Fig. 17. Unfortunately, a relation between the ideal and impact pressures in subsonic rarefied flows is not available, and correction for the pilot pressures is made only for the supersonic portion of the flow. It can be seen that the corrected DSMC pilot pressures show better agreement with the experimental data.

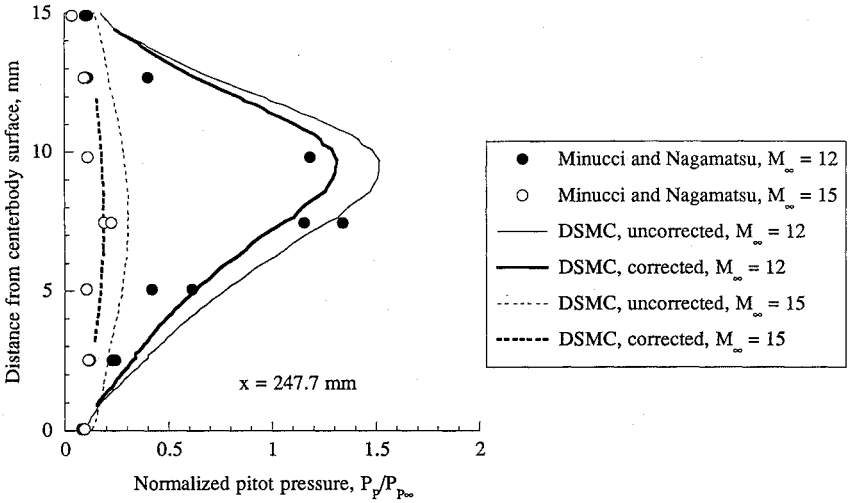

Fig. 17 Comparison of pitot pressure across the duct passage.

Conclusions

Hypersonic low-density flows around a scramjet inlet model have been analyzed using the DSMC method. Three hypersonic flow cases with different degrees of rarefaction are considered, which conventional continuum gasdynamics based on the concept of a local equilibrium may not be adequate to describe accurately. The present DSMC results show good agreement with the previous experimental data or theoretical solutions for similar wedge flow cases. However, some discrepancies between the DSMC results and the experimental data occur in the wall pressure along the centerbody surface near the leading edge of the ramp. Inside the duct passage, the DSMC results with an angle of attack of 2.5 deg give better agreement with the experiment. Comparison of the pitot pressure across the duct passage near the trailing edge of the duct shows reasonable agreement. Some discrepancies between the DSMC results and the experimental data may be attributed to three-dimensional effects and the orifice effect.

Acknowledgment

Support for the first author (C. Chung) by the NASA Lewis Research Center, Cleveland, Ohio, under Grant NCC 3-171 is gratefully acknowledged. Nan-Suey Liu is the grant director. The work of the second author (S. Kim) was supported by NASA Contract NAS 3-25266.

References

[1]Bird, G. A., *Molecular Gas Dynamics*, Oxford Univ. Press, London, 1976.

[2]Moss, J. N., Price, J. M., and Chun, Ch.-H., "Hypersonic Rarefied Flow About a Compression Corner—DSMC Simulation and Experiment," AIAA Paper 91-1313, June 1991.

[3]Carlson, A. B., and Wilmoth, R. G., "Monte Carlo Simulation of Near-Continuum Shock-Shock Interaction Problem," AIAA Paper 92-2862, July 1992.

[4]Minucci, M. A. S., and Nagamatsu, H. T., "Investigation of a Two-Dimensional Scramjet Inlet, M_∞ = 8–18 and T_0 = 4100 K," *Journal of Propulsion and Power*, Vol. 9, 1993.

[5]Lai, H. T., Kim, S. C., and Nagamatsu, H. T., "Calculation of Scramjet Inlet with Thick Boundary-Layer Ingestion," AIAA Paper 93-1836, June 1993.

[6]Pulliam, T. H., "Euler and Thin Layer Navier-Stokes Codes: ARC2D, ARC3D," Notes for Computational Fluid Dynamics User's Workshop, The University of Tennessee Space Institute, Tullahoma, TN, UTSI Publ. E02-4005-023084, May 1984, pp. 15.1–15.85.

[7]Cooper, G. K., "The PARC Code: Theory and Usage," Arnold Engineering Development Center, Arnold Air Force Station, TN, AEDC-TR-87-24, May 1987.

[8]Bird, G. A., "Monte Carlo Simulation in an Engineering Context," *Rarefied Gas Dynamics*, edited by S. S. Fisher, Vol. 74, Part I, Progress in Astronautics and Aeronautics, AIAA, New York, 1981, pp. 239–255.

[9]Bird, G. A., "The Perception of Numerical Methods in Rarefied Gas Dynamics," *Rarefied Gas Dynamics*, edited by E. P. Muntz, D. P. Weaver, and D. H. Campbell, Vol. 118, Progress in Astronautics and Aeronautics, AIAA, Washington, DC, 1989, pp. 211–226.

[10]Chung, C. H., Jeng, D. R., De Witt, K. J., and Keith, T. G. Jr., "Numerical Simulation of Rarefied Gas Flow through a Slit," *Journal of Thermophysics and Heat Transfer*, Vol. 6, No. 1, 1992, pp. 27–34.

[11]Chung, C. H., Kim, S. C., Stubbs, R. M., and De Witt, K. J., "DSMC and Continuum Analyses of Low Density Nozzle Flow," AIAA Paper 93-0727, Jan. 1993.

[12]Chung, C. H., Kim, S. C., Stubbs, R. M., and De Witt, K. J., "Analysis of Plume Backflow around a Nozzle Lip in a Nuclear Rocket," AIAA Paper 93-2497, June 1993.

[13]Usami, M., Fujimoto, T., and Kato, S., "Monte Carlo Simulation on Mass Flow Reduction Due to Roughness of a Slit Surface," *Rarefied Gas Dynamics*, edited by E. P. Muntz, D. P. Weaver, and D. H. Campbell, Vol. 116, Progress in Astronautics and Aeronautics, AIAA, Washington, DC, 1989, pp. 283–297.

[14]Boyd, I. D., "Vectorization of a Monte Carlo Simulation Scheme for Nonequilibrium Gas Dynamics," *Journal of Computational Physics*, Vol. 96, No. 2, Oct. 1991, pp. 411–427.

[15]McDonald, J. D., "A Computationally Efficient Particle Simulation Method Suited to Vector Computer Architectures," Ph.D. Thesis, Stanford Univ., Stanford, CA, Jan. 1990.

[16]Minucci, M. A. S., "An Experimental Investigation of a 2-D Scramjet Inlet at Flow Mach Numbers of 8 to 25 and Stagnation Temperatures of 800 to 4,100 K," Ph.D. Thesis, Rensselaer Polytechnic Inst., Troy, NY, May 1991.

[17]Borgnakke, C., and Larsen, P. S., "Statistical Collision Models for Monte Carlo Simulation of Polyatomic Gas Mixture," *Journal of Computational Physics*, Vol. 18, No. 4, Aug. 1975, pp. 405–420.

[18]Vidal, R. J., and Bartz, J. A., "Surface Measurements on Sharp Flat Plates and Wedges in Low-Density Hypersonic Flow," *AIAA Journal*, Vol. 7, No. 6, 1969, pp. 1099–1109.

[19]Chow, W. L., and Eilers, R. E., "Hypersonic Low-Density Flow past Slender Wedges," *AIAA Journal*, Vol. 67, No. 1, 1968, pp. 177–179.

[20]Potter, J. L., Kinslow, M., and Boylan, D. E., "An Influence of the Orifice on Measured Pressures in Rarefied Flow," *Rarefied Gas Dynamics*, Vol. II, edited by J. H. de Leeuw, Academic Press, New York, 1966, pp. 175–194.

[21]Harbour, P. J., and Bienkowski, G. K., "Methods for the Interpretation of Surface Pressure Measurements under Rarefied Hypersonic Conditions," *Physics of Fluids*, Vol. 16, No. 5, 1973, pp. 600–611.

[22]Fisher, S. S., "The Effect of Rarefaction on Impact Pressure Measurements in Supersonic Flows," *Rarefied Gas Dynamics*, Vol. 1, edited by O. M. Belolserkovskii, M. N. Kogan, S. S. Kutateladze, and A. K. Rebrov, Plenum Press, New York, 1985, pp. 461–468.